Computer Assisted Mechanics and Engineering Sciences, 8: 99–120, 2001.

Application of enthalpy formulations for numerical simulation of castings solidification

Norbert Sczygiol and Grzegorz Szwarc
Technical University of Częstochowa, Institute of Mechanics and Machine Design
ul. Dąbrowskiego 73, 42-200 Częstochowa, Poland

(Received September 29, 1999)

The paper deals with a numerical modelling of solidification in which enthalpy formulations were used. The finite element method (FEM) was applied for computer simulation of solidification. This is the most common numerical method used in the simulation of physical processes. The enthalpy formulations are more convenient to use than temperature formulations in the multidimensional problems in which FEM is applied. The paper concentrated on two enthalpy formulations: the apparent heat capacity formulation and the basic enthalpy formulation. The time integration schemes and the numerical realisation of boundary conditions were discussed. The models of solid phase growth and the implementation details used in this paper were shown in work [15]. The presented results of computer simulations contain: temperature fields, solidification kinetics, cooling velocities and calculated distributions of equiaxed grain size.

1. Introduction

Casting is one of the production methods for machine elements and equipment. The shapes and properties of cast products are formed when liquid metal is passing to the solid state. The pass from the liquid to the solid state is a process composed of many physical phenomena: heat flow, liquid metal movement, evolution of latent heat of solidification, diffusion and so on. Other phenomena, which have an influence mainly on functional value of casting and occur as a result of the phenomena mentioned above, also have major significance. They include: microstructure formation, stress formation, shrinkage and a variety of casting defects. If the description of the pass of metal from liquid to the solid state is being addressed on the macroscopic level then modelling of solidification takes place. If the description is being addressed on the microscopic level then modelling of crystallisation takes place.

Solidification can proceed at a constant temperature or at a range of temperatures. If solidification proceeds at a constant temperature (T_f) the so-called *Stefan problem* or *solidification problem with a zero-width interval of solidification temperatures* should be addressed. A sharp separation between liquid and solid phases occurs in the Stefan problem. The two phases are in contact with each other forming a solidification surface (front). The solidification of metal alloys generally proceeds at certain temperature intervals, so-called *temperature solidification intervals*. The initial stage of the solidification of an alloy is called the liquidus temperature (T_L), while the end of solidification is called the solidus temperature (T_S). There is no sharp separation between liquid and solid phases in this case as both phases are separated from each other by a so-called *mushy zone* (solidification front) in which both liquid and solid phases appear at the same time. The width of the mushy zone depends on the chemical constitution of the solidifying alloy and on the velocity of solidification (solid phase growth), and therefore on the conditions of carrying away heat. The occurrence of a mushy zone and its dynamics in the solidification process have an influence on the microstructure of the solidified metal.

The finite element method is most commonly used in numerical modelling and numerical simulation. The above method was also applied in this paper with special respect to its suitability

in connection with enthalpy formulations of solidification. One of those formulations, the so-called basic enthalpy formulation, directly takes the forming microstructure into account in the numerical model. This paper takes into consideration only the possibility of the formation of equiaxed microstructure.

2. The basic equations of the solidification process

Solidification is stated by a quasi-linear heat conduction equation containing the term of heat source, which describes the rate of latent heat evolution

$$\nabla \cdot (\lambda \nabla T) + \rho_s L \frac{\partial f_s}{\partial t} = c\rho \frac{\partial T}{\partial t}\,, \tag{1}$$

where λ is the thermal conductivity coefficient, c is the specific heat, ρ is the density (subscript s refers to the solid phase, l would denoted the liquid phase, f would denoted the pass from the liquid to the solid state), L is the latent heat of solidification and f_s is the solid phase fraction. These equations, together with suitable initial and boundary conditions (stated in Section 4) form the basis of the thermal description of solidification.

Taking into consideration the enthalpy, defined as follows,

$$H(T) = \int_{T_{\text{ref}}}^{T} c\rho(T)\, dT + \rho_s L\,(1 - f_s(T))\,, \tag{2}$$

where T_{ref} is the reference temperature and $c\rho$ is the heat capacity, one can pass to the so-called enthalpy description of the solidification process. A few types of enthalpy formulations of solidification exist. The prevailing ones are:

1. the apparent heat capacity formulation (AHC)

$$\nabla \cdot (\lambda \nabla T) = c^*(T) \frac{\partial T}{\partial t} \tag{3}$$

containing the effective heat capacity (c^*), which is obtained by differentiating Eq. (2) with respect to temperature

$$\frac{dH}{dT} = c\rho - \rho_s L \frac{\mathrm{d}f_s}{\mathrm{d}T} = c^*(T), \tag{4}$$

2. the basic enthalpy formulation (BEF)

$$\nabla \cdot (\lambda \nabla T) = \frac{\partial H}{\partial t}\,, \tag{5}$$

which is obtained by differentiating the enthalpy, given by Eq. (2), with respect to time

$$\frac{\partial H}{\partial t} = c\rho \frac{\partial T}{\partial t} - \rho_s L \frac{\partial f_s}{\partial t}\,, \tag{6}$$

3. the source enthalpy formulation

$$\nabla \cdot (\lambda \nabla T) + \rho_s L \frac{\partial f_s}{\partial t} = \frac{\partial h}{\partial t} \tag{7}$$

which is obtained by taking the source part from the total enthalpy and then by differentiating it with respect to time

$$\frac{\partial H}{\partial t} = \frac{\partial h}{\partial t} - \rho_s L \frac{\partial f_s}{\partial t}\,. \tag{8}$$

This formulation is very similar to the temperature description of solidification.

The first two formulations will be discussed in this paper in detail.

2.1. Enthalpy and the effective heat capacity

In the case of liquid metals or their alloys, the enthalpy contains both the apparent heat and the latent heat (latent heat of solidification). Using Eq. (2) for the Stefan problem, the enthalpy could be defined as follows [3, 18]

$$\begin{aligned} H &= \int_{T_{\text{ref}}}^{T} c\rho_s \, \mathrm{d}T, && \text{for } T < T_f, \\ H &= \int_{T_{\text{ref}}}^{T_f} c\rho_s \, \mathrm{d}T + \rho_s L + \int_{T_f}^{T} c\rho_l \, \mathrm{d}T, && \text{for } T > T_f \end{aligned} \tag{9}$$

(the subscripts refer to the $c\rho$ product), while for metal solidifying in the range (T_L–T_S) of temperatures, assuming that latent heat of solidification can be evaluated in an arbitrary way, the enthalpy is equal to [3, 18]

$$\begin{aligned} H &= \int_{T_{\text{ref}}}^{T} c\rho_s \, \mathrm{d}T, && \text{for } T < T_S, \\ H &= \int_{T_{\text{ref}}}^{T_S} c\rho_s \, \mathrm{d}T + \int_{T_S}^{T} \left(c\rho_f - \rho_s L \frac{\mathrm{d}f_s}{\mathrm{d}T} \right) dT, && \text{for } T_S \le T \le T_L, \\ H &= \int_{T_{\text{ref}}}^{T_S} c\rho_s \, \mathrm{d}T + \rho_s L + \int_{T_S}^{T_L} c\rho_f \, \mathrm{d}T + \int_{T_L}^{T} c\rho_l \, \mathrm{d}T, && \text{for } T > T_L. \end{aligned} \tag{10}$$

The heat capacity expression is obtained by differentiating the enthalpy with respect to temperature. After differentiating Eq. (9) one can obtain

$$\begin{aligned} c^* &= c\rho_s, && \text{for } T < T_S, \\ c^* &= c\rho_l, && \text{for } T > T_L. \end{aligned} \tag{11}$$

In the same way, after differentiating Eq. (10) one can obtain

$$\begin{aligned} c^* &= c\rho_s, && \text{for } T < T_S, \\ c^* &= c\rho_f - \rho_s L \frac{\mathrm{d}f_s}{\mathrm{d}T}, && \text{for } T_S \le T \le T_L, \\ c^* &= c\rho_l, && \text{for } T > T_L. \end{aligned} \tag{12}$$

Equations (9) and (10) as well as (11) and (12) show that the courses of relationship of enthalpy and effective heat capacity to temperature are different for pure metals (Fig. 1) and metal alloys (Fig. 2). The above comparison shows that numerical calculation of the enthalpy derivative with respect to temperature for metal alloys that solidify at a range of temperatures should not provide any numerical problems, while calculating the same derivative for pure metals or metal alloys solidifying at a constant temperature is not possible. The enthalpy formulations of solidification need a different approach to solidification modelling at a constant temperature [6]. The above problem is solved by substituting the solidification at a constant temperature with the solidification in a very narrow range of temperatures [3, 16, 18].

The detailed description of the course of enthalpy shown in Fig. 2 requires enthalpy values to be given for certain characteristic temperatures. These values can be calculated from relationship (10). By assuming that the heat capacity of the transient zone, which contains liquid and solid phases, is the following arithmetic average

$$c\rho_f = \frac{1}{2}(c\rho_s + c\rho_l), \tag{13}$$

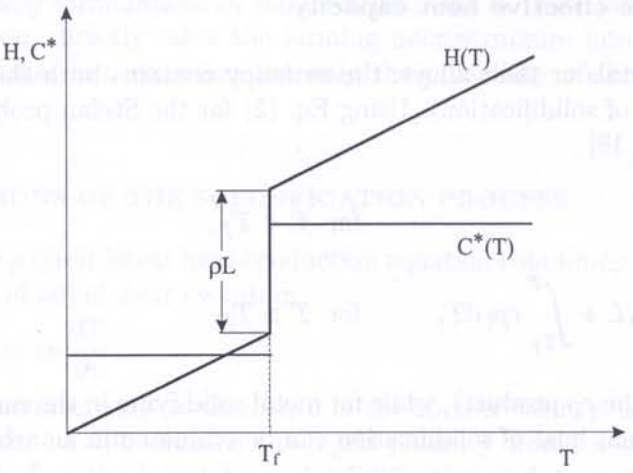

Fig. 1. The functions of enthalpy and effective heat capacity for pure metal

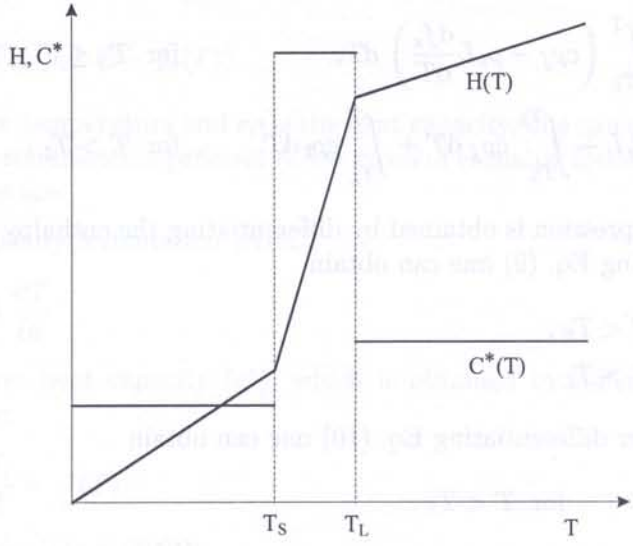

Fig. 2. The functions of enthalpy and effective heat capacity for metal alloy

one can obtain

$$
\begin{aligned}
H &= c\rho_s T\,, && \text{for } T < T_S\,,\\
H &= c\rho_s T_S\,, && \text{for } T = T_S\,,\\
H &= c\rho_s T_S + \rho_s L + \frac{1}{2}(c\rho_s + c\rho_l)(T_L - T_S), && \text{for } T = T_L\,,\\
H &= c\rho_s T_S + \rho_s L + \frac{1}{2}(c\rho_s + c\rho_l)(T_L - T_S) + c\rho_l(T - T_L), && \text{for } T > T_L\,.
\end{aligned}
\tag{14}
$$

The linear relationship between enthalpy and temperature is assumed between T_L and T_S temperatures.

3. Numerical models of solidification

The models describing particular formulations are transformed using the finite element method to build an algebraic system of equations. The semi-discretisation (discretisation only over the space)

gives the ordinary differential equations with the time derivatives. In the next stage, that is to say discretisation over time, the above equations are rearranged into algebraic systems of equations for single finite elements. The global system of equations is obtained as a result of assembling all the finite elements of the task.

The discretisation over time is carried out with one- and two-steps schemes in the numerical modelling of solidification [3, 16, 18]. Θ scheme is one of the one-step schemes, and has the following form [19],

$$u^{n+1} = u^n + \Delta t \left[(1-\Theta)\mathcal{L}u^n + \Theta \mathcal{L}u^{n+1}\right], \tag{15}$$

where u is the integrated quantity, Δt is the time step, $\mathcal{L}u$ is the derivative of the integrated quantity with respect to time, obtained as a result of semi-discretisation, while superscript n refers to the successive integration steps over time. The two-step scheme can be written as [19]

$$\alpha u^{n+2} + (1-2\alpha)u^{n+1} + (\alpha - 1)u^n = \Delta t\left[\beta \mathcal{L}u^{n+2} + \left(\frac{1}{2} + \alpha - 2\beta\right)\mathcal{L}u^{n+1} + \left(\frac{1}{2} - \alpha + \beta\right)\mathcal{L}u^n\right] \tag{16}$$

where α and β coefficients must fulfil the conditions of solution stability.

In this work two schemes of time integration are used; the Euler backward scheme (one-step) and Dupont II scheme (two-step). The Euler backward scheme (EB) is obtained after substituting $\Theta = 1$ in Eq. (16)

$$u^{n+1} = u^n + \Delta t\, \mathcal{L}u^{n+1} \tag{17}$$

while Dupont II scheme takes the form

$$u^{n+2} - u^{n+1} = \Delta t\left[\left(\tfrac{1}{2} + a\right)\mathcal{L}u^{n+2} + \left(\tfrac{1}{2} - 2a\right)\mathcal{L}u^{n+1} + a\mathcal{L}u^{n}.\right]. \tag{18}$$

Coefficient a is chosen experimentally. The best results are obtained for $a = \frac{1}{4}$ [3].

3.1. The apparent heat capacity formulation

The semi-discretisation of Eq. (3) gives as a result [11]

$$\mathbf{M}(T)\dot{\mathbf{T}} + \mathbf{K}(T)\mathbf{T} = \mathbf{b}(T) \tag{19}$$

while

$$\mathbf{M} = \int_\Omega c^* \mathbf{N}^T \mathbf{N}\, \mathrm{d}\Omega, \tag{20}$$

$$\mathbf{K} = \int_\Omega \lambda \nabla^T \mathbf{N} \cdot \nabla \mathbf{N}\, \mathrm{d}\Omega, \tag{21}$$

$$\mathbf{b} = \int_\Gamma \mathbf{N}_\Gamma^T \mathbf{N}_\Gamma\, \mathrm{d}\Gamma\, \mathbf{q}^T, \tag{22}$$

where $\mathbf{M}$ is the mass matrix, $\mathbf{K}$ is the conductivity matrix, $\mathbf{T}$ is the temperature vector and $\mathbf{b}$ is the right-hand side vector, whose values are calculated on the boundary conditions basis, while $\mathbf{N}$ is the shape function vector in the Ω domain, $\mathbf{N}_\Gamma$ is the shape function vector on the Γ boundary and $\mathbf{q}$ is the vector of nodal heat fluxes.

For the Euler backward scheme Eq. (19) takes the form [12]

$$\left(\mathbf{M}^{n+1} + \Delta t\, \mathbf{K}^{n+1}\right)\mathbf{T}^{n+1} = \mathbf{M}^n \mathbf{T}^n + \Delta t\, \mathbf{b}^{n+1} \tag{23}$$

while for Dupont II scheme one can obtain

$$\left(\mathbf{M}^0 + \frac{3}{4}\Delta t\mathbf{K}^0\right)\mathbf{T}^{n+2} = \mathbf{M}^0\mathbf{T}^{n+1} - \frac{1}{4}\Delta t\,\mathbf{K}^0\mathbf{T}^n + \frac{3}{4}\Delta t\,\mathbf{b}^{n+2} + \frac{1}{4}\Delta t\,\mathbf{b}^n. \tag{24}$$

Superscript $(^0)$ denotes that material properties are calculated for extrapolated temperature according to the equation

$$T = \frac{3}{2}T^{n+1} - \frac{1}{2}T^n. \tag{25}$$

The effective heat capacity is present in the mass matrix in the above formulation. It is calculated as an enthalpy derivative with respect to temperature (see Eq. (4)). However, because the simple differential approximation can lead to considerable numerical errors and the oscillation of the solution [3], the derivative needs suitable approximation. A few schemes of approximation of effective heat capacity exist [1, 3, 18]. In this paper the Del Giudice scheme [3] is used, in which

$$c^* = \frac{H_{,\alpha}T_{,\alpha}}{T_{,\beta}T_{,\beta}} \tag{26}$$

where α and β are space coordinates. When enthalpies and temperatures are expressed by their values in finite element nodes and shape functions

$$H = H_i N_i\,, \qquad T = T_i N_i\,, \tag{27}$$

where $i = 1 \ldots w$, and w is the number of nodes in a particular finite element, one can obtain

$$c^* = \frac{H_i N_{i,\alpha} T_j N_{j,\alpha}}{T_k N_{k,\beta} T_l N_{l,\beta}}\,. \tag{28}$$

It must be borne in mind that the sum of shape function derivatives is equal to zero, which could lead to indeterminacy.

3.2. The basic enthalpy formulation

The semi-discretisation of Eq. (5) gives [11]

$$\mathbf{M}\dot{\mathbf{H}} + \mathbf{K}(T)\mathbf{T} = \mathbf{b}(T), \tag{29}$$

where $\mathbf{H}$ is the enthalpy vector. For this formulation the mass matrix is calculated according to the equation

$$\mathbf{M} = \int_\Omega \mathbf{N}^T\mathbf{N}\,\mathrm{d}\Omega, \tag{30}$$

while the conductivity matrix and right-hand side vector are calculated according to Eqs. (21) and (22).

For the Euler backward scheme Eq. (29) takes the form [12]

$$\mathbf{M}\mathbf{H}^{n+1} + \Delta t\,\mathbf{K}^{n+1}\mathbf{T}^{n+1} = \mathbf{M}\mathbf{H}^n + \Delta t\,\mathbf{b}^{n+1}, \tag{31}$$

while for Dupont II scheme

$$\mathbf{M}\mathbf{H}^{n+2} + \frac{3}{4}\Delta t\,\mathbf{K}^0\mathbf{T}^{n+2} = \mathbf{M}\mathbf{H}^n - \frac{1}{4}\Delta t\,\mathbf{K}^0\mathbf{T}^n + \frac{3}{4}\Delta t\,\mathbf{b}^{n+2} + \frac{1}{4}\Delta t\,\mathbf{b}^n. \tag{32}$$

The superscript $(^0)$ refers to material properties determined for the temperature according to Eq. (25). Enthalpy and temperature are on the same time level in the last two equations. The enthalpy is the basic quantity in that formulation, so temperature on the time level $n+1$ (in Eq. (31))

and $n+2$ (in Eq. (32)) should be substituted by some other quantities. The temperatures can be expanded in Taylor series. The first two terms of that expansion are as follows

$$\mathbf{T}^{n+\alpha+1} = \mathbf{T}^{n+\alpha} + \left[\frac{\mathrm{d}\mathbf{T}}{\mathrm{d}\mathbf{H}}\right]^{n+\alpha} \Delta\mathbf{H}, \tag{33}$$

while

$$\Delta\mathbf{H} = \mathbf{H}^{n+\alpha+1} - \mathbf{H}^{n+\alpha}, \tag{34}$$

where α takes 0 value for the time level $n+1$ and 1 for time level $n+2$. The temperature derivative with respect to enthalpy is the diagonal matrix. In the Euler backward scheme by assuming that the conductivity matrix is determined on the time level n $\left(\mathbf{K}^{n+1} \to \mathbf{K}^{n}\right)$, one can obtain

$$\left(\mathbf{M} + \Delta t\,\mathbf{K}^{n}\left[\frac{\mathrm{d}\mathbf{T}}{\mathrm{d}\mathbf{H}}\right]^{n}\right)\mathbf{H}^{n+1} = \left(\mathbf{M} + \Delta t\,\mathbf{K}^{n}\left[\frac{\mathrm{d}\mathbf{T}}{\mathrm{d}\mathbf{H}}\right]^{n}\right)\mathbf{H}^{n} - \Delta t\,\mathbf{K}^{n}\mathbf{T}^{n} + \Delta t\,\mathbf{b}^{n+1}. \tag{35}$$

The final form of the matrix equation for Dupont II scheme is obtained by substituting Eqs. (33) and (34) into Eq. (32)

$$\left(\mathbf{M} + \frac{3}{4}\Delta t\,\mathbf{K}^{0}\left[\frac{\mathrm{d}\mathbf{T}}{\mathrm{d}\mathbf{H}}\right]^{n+1}\right)\mathbf{H}^{n+2} = \left(\mathbf{M} + \frac{3}{4}\Delta t\,\mathbf{K}^{0}\left[\frac{\mathrm{d}\mathbf{T}}{\mathrm{d}\mathbf{H}}\right]^{n+1}\right)\mathbf{H}^{n+1} - \frac{3}{4}\Delta t\,\mathbf{K}^{0}\mathbf{T}^{n+1} - \frac{1}{4}\Delta t\,\mathbf{K}^{0}\mathbf{T}^{n} + \frac{3}{4}\Delta t\,\mathbf{b}^{n+2} + \frac{1}{4}\Delta t\,\mathbf{b}^{n}. \tag{36}$$

The product of the symmetrical conductivity matrix $\mathbf{K}$ and diagonal matrix $\mathrm{d}\mathbf{T}/\mathrm{d}\mathbf{H}$, occurring in Eqs. (35) and (36), is an asymmetrical matrix. As a result the global matrix of coefficients in the system of equations is an asymmetrical matrix, too. This inconvenience can be avoided by averaging the coefficients of the diagonal matrix. However, because the introduction of boundary conditions of the fourth type also leads to a loss of symmetry in the global matrix of coefficients (see Section 4), the averaging of coefficients of the diagonal matrix $\mathrm{d}\mathbf{T}/\mathrm{d}\mathbf{H}$ is not carried out.

The coefficients of the diagonal matrix $\mathrm{d}\mathbf{T}/\mathrm{d}\mathbf{H}$ are calculated on the basis of equations obtained as a result of differentiating expressions (10) with respect to temperature. The transformation of Eq. (12) leads to

$$\begin{aligned}
&\frac{\mathrm{d}T}{\mathrm{d}H} = \frac{1}{c\rho_s}, && \text{for } T < T_S,\\
&\frac{\mathrm{d}T}{\mathrm{d}H} = \frac{1}{c\rho_f - \rho_s L\frac{\mathrm{d}f_s}{\mathrm{d}T}}, && \text{for } T_S \le T \le T_L,\\
&\frac{\mathrm{d}T}{\mathrm{d}H} = \frac{1}{c\rho_l}, && \text{for } T > T_L.
\end{aligned} \tag{37}$$

It should be noted that the application of the above expression in Eqs. (35) and (36) requires a knowledge of the relationship of the solid phase fraction to temperature. However, it is possible to take the forming microstructure directly into account in the above formulation. For two-component metal alloys, if the possibility of solute diffusion in the solid phase is assumed, and perfect solute solubility takes place in the liquid phase [7], then the solid phase growth is given by the relationship [8, 13, 15]

$$f_s(T) = \frac{1}{1-nk\alpha}\left(1 - \left(\frac{T_M - T}{T_M - T_L}\right)^{\frac{1-nk\alpha}{k-1}}\right), \tag{38}$$

where

$$\alpha = \frac{D_s}{r_g^2} t_f \tag{39}$$

and D_s is the solute diffusion coefficient in the solid phase, t_f is the so-called local solidification time, r_g is the characteristic grain size and n is a coefficient engaging the grain shape ($n = 2$ for plane grain (plate), $n = 4$ for cylindrical grain and $n = 6$ for spherical grain). The relationship of solid phase fraction for both equilibrium and non-equilibrium solidification models [13] can be educed from Eq. (38).

3.3. Comments on the assembly and solution of the system of equations

Equations (23) and (24), discussed above, for the apparent heat capacity formulation, and Eqs. (35) and (36), for the basic enthalpy formulation, serve to create a system of equations for finite element meshes. The finite element meshes discretise the analysed regions. The systems of equations, completed with the boundary conditions, are solved with appropriate methods. However, because the system of equations are usually very large, iterative methods are applied to solve them. For both solidification formulations discussed in this paper, different solution methods for the system of equations should be used. In the case of the apparent heat capacity formulation, where the coefficient matrix is symmetrical, the conjugate gradients method can be applied. In the case of the basic enthalpy formulation, where the coefficient matrix is asymmetrical, the bi-conjugate gradients method can be applied. In both cases suitable preconditioning methods are used to accelerate the solution convergence [10].

The coefficients matrix of the system of equations is created from the mass matrix and conductivity matrix. For small time steps, temperature (or enthalpy) oscillations could sometimes be obtained. These oscillations can occur near the regions contact places, where there are considerable temperature differences, e.g. the contact of the alloy with the mould, the contact of the alloy with the environment and near the mushy zone [2, 3]. The diagonalisation of the mass matrix is the most effective method of avoiding those oscillations in the numerical solutions. It is especially easy for triangular elements [19], but extra calculations for quadrilateral elements are needed.

4. THE NUMERICAL REALISATION OF BOUNDARY CONDITIONS

The boundary conditions can be constant or can change during the solidification process and cooling of the casting. The variability of boundary conditions can be caused by the fact that material properties can depend on some parameters of the process, i.e. temperature. One can distinguish four types of boundary condition in the modelling of solidification, these are the same as those found in thermal conductivity modelling:

1. the boundary condition of the first type (Dirichlet condition), where the temperature (T_{giv}) is given on the Γ boundary of Ω domain

$$\Gamma: \quad T = T_{\text{giv}}(t), \tag{40}$$

2. the boundary condition of the second type (Neumann condition), where the heat flux (q_{giv}) is given on the Γ boundary of Ω domain

$$\Gamma: \quad q = q_{\text{giv}}(t), \tag{41}$$

3. the boundary condition of the third type (Newton condition), where heat exchange with environment takes place on the Γ boundary of Ω domain

$$\Gamma: \quad q = \alpha(T)(T_{|\Gamma} - T_{\text{env}}(t)), \tag{42}$$

where α is the heat exchange coefficient with the environment, $T_{|\Gamma}$ is the temperature on the boundary Γ of the domain and T_{env} is the ambient temperature. The heat radiation, which

performs a crucial role when the mould cavity is filled with the melt, is introduced to the mathematical description through the above boundary condition. In this case the α coefficient is composed of two parts: convectional and radiant,

4. the boundary condition of the fourth type (continuity condition), on the Γ boundary, which separates Ω_1 and Ω_2 domains, where the heat flow takes place

$$\Gamma: \begin{cases} -\lambda_1 \dfrac{\partial T^{(1)}}{\partial n} = -\lambda_2 \dfrac{\partial T^{(2)}}{\partial n} = \dfrac{\beta}{\delta}\left(T^{(1)} - T^{(2)}\right), \\ T^{(1)} \neq T^{(2)}, \end{cases} \tag{43}$$

where β is the thermal conductivity coefficient of the material in the separating layer, δ is the thickness of this layer and $\mathbf{n}$ is the normal vector to the boundary. If there is no separating layer between these two subdomains, then $T^{(1)} = T^{(2)}$.

The boundary conditions, apart from the first type, are introduced into the global system of equations through Eq. (22). The boundary shape functions, which depend on the type of finite elements, should be replaced in the integrand of the above equation. When modelling two-dimensional problems using linear finite elements, expression (22) takes the following form for the local numbering of nodes

$$\begin{Bmatrix} b_1 \\ b_2 \end{Bmatrix} = \frac{h}{6} \begin{bmatrix} 2 & 1 \\ 1 & 2 \end{bmatrix} \begin{Bmatrix} q_1 \\ q_2 \end{Bmatrix}, \tag{44}$$

where h is the distance between nodes on the boundary and subscripts 1 and 2 refer to the indices of nodes in local numbering (Fig. 3).

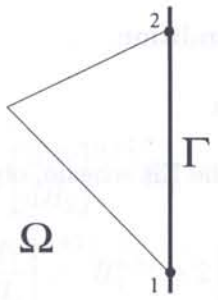

Fig. 3. Local boundary discretisation

The boundary conditions are introduced for the Euler backward scheme on the $n+1$ time level, while for Dupont II on the n and $n+2$ time levels

$$\mathbf{b} = \begin{cases} \mathbf{b}^{n+1}, & \text{for Euler backward scheme,} \\ \dfrac{3}{4}\mathbf{b}^{n+2} + \dfrac{1}{4}\mathbf{b}^{n}, & \text{for Dupont II scheme.} \end{cases} \tag{45}$$

The way of introducing the boundary condition of the first type into the global system of equations is the same in both solidification formulations and time integration schemes considered here. The temperatures are introduced in the apparent heat capacity formulation, while enthalpies are introduced in the basic enthalpy formulation. The second type of boundary condition is introduced in both time integration schemes in the same way. The third and fourth type of boundary conditions are introduced in both solidification formulations and both time integration schemes in different ways. However, it should also be noted that the application of the fourth type of boundary condition causes a loss of symmetry in the coefficient matrix in the basic enthalpy formulation. This effect doesn't occur in the apparent heat capacity formulation.

4.1. The first type of boundary condition

The introduction of the first type of boundary condition relies on suitable modification in the right-hand side vector and in the global coefficient matrix. This means that **b** vector, defined by Eq. (45), is not introduced into the global system of equations in this case. The modification of the coefficient matrix relies on putting the value 1 on the main diagonal in the equation where the number corresponds to the node number on the boundary, and then transferring every coefficient from the column with the same number — multiplied by a given temperature (for AHC) or enthalpy (for BEF) — to the right-hand side of the system of equations, and finally putting the value 0 in their places, in both the row and column. The modification of the right-hand side vector relies on putting the given temperature value (AHC) or enthalpy (BEF) to the right-hand side of the equation where the number corresponds to the node number on the boundary.

4.2. The second type of boundary condition

Only the modification of the right-hand side vector proceeds independently of the type of solidification formulation or time integration scheme. By assuming that a different value of heat flux is given in every boundary node, the above modification equals

$$\begin{aligned} b_1 &= \frac{h}{6}(2q_1 + q_2), \\ b_2 &= \frac{h}{6}(q_1 + 2q_2). \end{aligned} \tag{46}$$

4.3. The third type of boundary condition

Apparent heat capacity formulation

Substituting Eq. (42) into Eq. (44) for the EB scheme, obtains

$$\begin{aligned} b_1 &= \frac{h\alpha}{6}(-2T_1^{n+1} - T_2^{n+1} + 3T_{\text{env}}), \\ b_2 &= \frac{h\alpha}{6}(-T_1^{n+1} - 2T_2^{n+1} + 3T_{\text{env}}). \end{aligned} \tag{47}$$

While for Dupont II scheme, according to Eq. (45), fluxes (42) should be substituted into Eq. (44) for n and $n+2$ time steps. This obtains

$$\begin{aligned} b_1 &= \frac{3}{4}\frac{h\alpha}{6}(-2T_1^{n+2} - T_2^{n+2}) + \frac{3}{4}\frac{h\alpha}{6}3T_{\text{env}} + \frac{1}{4}\frac{h\alpha}{6}(-2T_1^{n} - T_2^{n} + 3T_{\text{env}}), \\ b_2 &= \frac{3}{4}\frac{h\alpha}{6}(-T_1^{n+2} - 2T_2^{n+2}) + \frac{3}{4}\frac{h\alpha}{6}3T_{\text{env}} + \frac{1}{4}\frac{h\alpha}{6}(-T_1^{n} - 2T_2^{n} + 3T_{\text{env}}). \end{aligned} \tag{48}$$

Basic enthalpy formulation

For EB scheme, as for the apparent heat capacity formulation, we have

$$\begin{aligned} b_1 &= \frac{h\alpha}{6}(-2T_1^{n+1} - T_2^{n+1} + 3T_{\text{env}}), \\ b_2 &= \frac{h\alpha}{6}(-T_1^{n+1} - 2T_2^{n+1} + 3T_{\text{env}}). \end{aligned} \tag{49}$$

Substituting Eqs. (33) and (34) into the above equations leads to

$$b_1 = -\frac{2h\alpha}{6}\left[\frac{\mathrm{d}T_1}{\mathrm{d}H_1}\right]^n H_1^{n+1} - \frac{h\alpha}{6}\left[\frac{\mathrm{d}T_2}{\mathrm{d}H_2}\right]^n H_2^{n+1} + \frac{h\alpha}{6}\left(-2T_1^n - T_2^n + 3T_{\mathrm{env}} + 2\left[\frac{\mathrm{d}T_1}{\mathrm{d}H_1}\right]^n H_1^n + \left[\frac{\mathrm{d}T_2}{\mathrm{d}H_2}\right]^n H_2^n\right) \tag{50}$$

and

$$b_2 = -\frac{h\alpha}{6}\left[\frac{\mathrm{d}T_1}{\mathrm{d}H_1}\right]^n H_1^{n+1} - \frac{2h\alpha}{6}\left[\frac{\mathrm{d}T_2}{\mathrm{d}H_2}\right]^n H_2^{n+1} + \frac{h\alpha}{6}\left(-T_1^n - 2T_2^n + 3T_{\mathrm{env}} + \left[\frac{\mathrm{d}T_1}{\mathrm{d}H_1}\right]^n H_1^n + 2\left[\frac{\mathrm{d}T_2}{\mathrm{d}H_2}\right]^n H_2^n\right). \tag{51}$$

On the basis of Eq. (45) for Dupont II scheme, it can be written

$$\begin{aligned} b_1 &= \frac{3}{4}\frac{h\alpha}{6}(-2T_1^{n+2} - T_2^{n+2} + 3T_{\mathrm{env}}) + \frac{1}{4}\frac{h\alpha}{6}(-2T_1^n - T_2^n + 3T_{\mathrm{env}}), \\ b_2 &= \frac{3}{4}\frac{h\alpha}{6}(-T_1^{n+2} - 2T_2^{n+2} + 3T_{\mathrm{env}}) + \frac{1}{4}\frac{h\alpha}{6}(-T_1^n - 2T_2^n + 3T_{\mathrm{env}}). \end{aligned} \tag{52}$$

Substituting Eqs. (33) and (34) into Eq. (52) obtains

$$b_1 = -\frac{3}{4}\frac{h\alpha}{6}2\left[\frac{\mathrm{d}T_1}{\mathrm{d}H_1}\right]^{n+1} H_1^{n+2} - \frac{3}{4}\frac{h\alpha}{6}\left[\frac{\mathrm{d}T_2}{\mathrm{d}H_2}\right]^{n+1} H_2^{n+2} + \frac{3}{4}\frac{h\alpha}{6}\left(-2T_1^{n+1} - T_2^{n+1} + 2\left[\frac{\mathrm{d}T_1}{\mathrm{d}H_1}\right]^{n+1} H_1^{n+1} + \left[\frac{\mathrm{d}T_2}{\mathrm{d}H_2}\right]^{n+1} H_2^{n+1} + 3T_{\mathrm{env}}\right) + \frac{1}{4}\frac{h\alpha}{6}(-2T_1^n - T_2^n + 3T_{\mathrm{env}}) \tag{53}$$

and

$$b_2 = -\frac{3}{4}\frac{h\alpha}{6}\left[\frac{\mathrm{d}T_1}{\mathrm{d}H_1}\right]^{n+1} H_1^{n+2} - \frac{3}{4}\frac{h\alpha}{6}2\left[\frac{\mathrm{d}T_2}{\mathrm{d}H_2}\right]^{n+1} H_2^{n+2} + \frac{3}{4}\frac{h\alpha}{6}\left(-T_1^{n+1} - 2T_2^{n+1} + \left[\frac{\mathrm{d}T_1}{\mathrm{d}H_1}\right]^{n+1} H_1^{n+1} + 2\left[\frac{\mathrm{d}T_2}{\mathrm{d}H_2}\right]^{n+1} H_2^{n+1} + 3T_{\mathrm{env}}\right) + \frac{1}{4}\frac{h\alpha}{6}(-T_1^n - 2T_2^n + 3T_{\mathrm{env}}). \tag{54}$$

4.4. The fourth type of boundary condition

If Ω_1 and Ω_2 domains are separated from each other by a certain layer, then that layer can be covered by a finite elements mesh. The separating layers are normally very thin (in comparison to casting or mould dimensions) so the generation of finite elements is difficult in them. The application of a virtual separating layer characterised by heat exchange coefficient κ is a more effective solution. However, while the finite element nodes in the contacting domains can have the same coordinates, they must have different indices. The local numbering of nodes in elements which are in contact is shown in Fig. 4. The coordinates of nodes 1 and 3 as well as 2 and 4 are the same in the finite element mesh. These meshes are easier for automatic generation.

The heat fluxes flowing through the virtual separating layer equal

$$\begin{aligned} q_1 &= -\kappa(T_1 - T_3), \\ q_2 &= -\kappa(T_2 - T_4). \end{aligned} \tag{55}$$

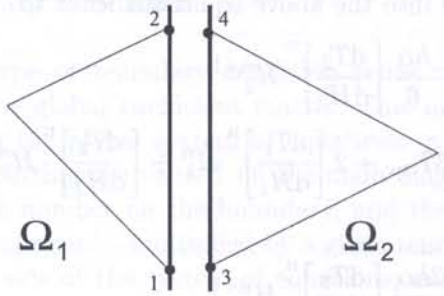

Fig. 4. Local discretisation of two contacting domains

Apparent heat capacity formulation

The equations for the Euler backward scheme are obtained by substituting Eq. (55) into Eq. (44)

$$\begin{aligned} b_1 &= -\frac{h\kappa}{6}(2T_1^{n+1} + T_2^{n+1} - 2T_3^{n+1} - T_4^{n+1}), \\ b_2 &= -\frac{h\kappa}{6}(T_1^{n+1} + 2T_2^{n+1} - T_3^{n+1} - 2T_4^{n+1}), \end{aligned} \tag{56}$$

while for Dupont II scheme we have

$$\begin{aligned} b_1 &= \frac{3}{4}\frac{h\kappa}{6}(-2T_1^{n+2} + 2T_3^{n+2} - T_2^{n+2} + T_4^{n+2}) - \frac{1}{4}\frac{h\kappa}{6}(2T_1^n - 2T_3^n + T_2^n - T_4^n), \\ b_2 &= \frac{3}{4}\frac{h\kappa}{6}(-T_1^{n+2} + T_3^{n+2} - 2T_2^{n+2} + 2T_4^{n+2}) - \frac{1}{4}\frac{h\kappa}{6}(T_1^n - T_3^n + 2T_2^n - 2T_4^n). \end{aligned} \tag{57}$$

Basic enthalpy formulation

The relationships (56) are also valid for the Euler backward scheme, but Eqs. (33) and (34) should now be substituted into them. This obtains

$$\begin{aligned} b_1 = -\frac{h\kappa}{6}\Bigg(&2\left[\frac{\mathrm{d}T_1}{\mathrm{d}H_1}\right]^n H_1^{n+1} + \left[\frac{\mathrm{d}T_2}{\mathrm{d}H_2}\right]^n H_2^{n+1} - 2\left[\frac{\mathrm{d}T_3}{\mathrm{d}H_3}\right]^n H_3^{n+1} - \left[\frac{\mathrm{d}T_4}{\mathrm{d}H_4}\right]^n H_4^{n+1} \\ &- 2\left[\frac{\mathrm{d}T_1}{\mathrm{d}H_1}\right]^n H_1^n - \left[\frac{\mathrm{d}T_2}{\mathrm{d}H_2}\right]^n H_2^n + 2\left[\frac{\mathrm{d}T_3}{\mathrm{d}H_3}\right]^n H_3^n + \left[\frac{\mathrm{d}T_4}{\mathrm{d}H_4}\right]^n H_4^n + 2T_1^n + T_2^n - 2T_3^n - T_4^n\Bigg) \end{aligned} \tag{58}$$

and

$$\begin{aligned} b_2 = -\frac{h\kappa}{6}\Bigg(&\left[\frac{\mathrm{d}T_1}{\mathrm{d}H_1}\right]^n H_1^{n+1} + 2\left[\frac{\mathrm{d}T_2}{\mathrm{d}H_2}\right]^n H_2^{n+1} - \left[\frac{\mathrm{d}T_3}{\mathrm{d}H_3}\right]^n H_3^{n+1} - 2\left[\frac{\mathrm{d}T_4}{\mathrm{d}H_4}\right]^n H_4^{n+1} \\ &- \left[\frac{\mathrm{d}T_1}{\mathrm{d}H_1}\right]^n H_1^n - 2\left[\frac{\mathrm{d}T_2}{\mathrm{d}H_2}\right]^n H_2^n + \left[\frac{\mathrm{d}T_3}{\mathrm{d}H_3}\right]^n H_3^n + 2\left[\frac{\mathrm{d}T_4}{\mathrm{d}H_4}\right]^n H_4^n + T_1^n + 2T_2^n - T_3^n - 2T_4^n\Bigg). \end{aligned} \tag{59}$$

The relationships (57) are also obtained for Dupont II scheme according to Eqs. (45) and (55).

Substituting Eqs. (33) and (34) into Eqs. (58) and (59) finally obtains

$$b_1 = -\frac{3}{4}\frac{h\kappa}{6}\left(2\left[\frac{\mathrm{d}T_1}{\mathrm{d}H_1}\right]^{n+1} H_1^{n+2} + \left[\frac{\mathrm{d}T_2}{\mathrm{d}H_2}\right]^{n+1} H_2^{n+2} - 2\left[\frac{\mathrm{d}T_3}{\mathrm{d}H_3}\right]^{n+1} H_3^{n+2} - \left[\frac{\mathrm{d}T_4}{\mathrm{d}H_4}\right]^{n+1} H_4^{n+2} - 2\left[\frac{\mathrm{d}T_1}{\mathrm{d}H_1}\right]^{n+1} H_1^{n+1} - \left[\frac{\mathrm{d}T_2}{\mathrm{d}H_2}\right]^{n+1} H_2^{n+1} + 2\left[\frac{\mathrm{d}T_3}{\mathrm{d}H_3}\right]^{n+1} H_3^{n+1} + \left[\frac{\mathrm{d}T_4}{\mathrm{d}H_4}\right]^{n+1} H_4^{n+1} + 2T_1^{n+1} + T_2^{n+1} - 2T_3^{n+1} - T_4^{n+1}\right) - \frac{1}{4}\frac{h\kappa}{6}\left(2T_1^n + T_2^n - 2T_3^n - T_4^n\right) \tag{60}$$

and

$$b_2 = -\frac{3}{4}\frac{h\kappa}{6}\left(\left[\frac{\mathrm{d}T_1}{\mathrm{d}H_1}\right]^{n+1} H_1^{n+2} + 2\left[\frac{\mathrm{d}T_2}{\mathrm{d}H_2}\right]^{n+1} H_2^{n+2} - \left[\frac{\mathrm{d}T_3}{\mathrm{d}H_3}\right]^{n+1} H_3^{n+2} - 2\left[\frac{\mathrm{d}T_4}{\mathrm{d}H_4}\right]^{n+1} H_4^{n+2} - \left[\frac{\mathrm{d}T_1}{\mathrm{d}H_1}\right]^{n+1} H_1^{n+1} - 2\left[\frac{\mathrm{d}T_2}{\mathrm{d}H_2}\right]^{n+1} H_2^{n+1} + \left[\frac{\mathrm{d}T_3}{\mathrm{d}H_3}\right]^{n+1} H_3^{n+1} + 2\left[\frac{\mathrm{d}T_4}{\mathrm{d}H_4}\right]^{n+1} H_4^{n+1} + T_1^{n+1} + 2T_2^{n+1} - T_3^{n+1} - 2T_4^{n+1}\right) - \frac{1}{4}\frac{h\kappa}{6}\left(T_1^n + 2T_2^n - T_3^n - 2T_4^n\right). \tag{61}$$

Equations (56), (58), (59), (60) and (61) are valid for Ω_1 domain, which contains boundary nodes 1 and 2. Analogous equations, as mentioned above, are used for Ω_2 domain, which contains boundary nodes 3 and 4, but the signs in these equations must be reversed. As a result, from the formula for b_1 one can obtain a formula for b_3, while from the formula for b_2 one can obtain a formula for b_4.

5. THE MODELLING OF EQUIAXED MICROSTRUCTURE

To simulate the numerical microstructure formed in castings is one of the most difficult tasks in the computer simulation of solidification. The extent of zones with different types of microstructure as well as the characteristic dimensions of grains in these zones, depend on the degree of undercooling of the melt at the beginning of solidification [5, 9, 17]. The undercooling depends on the velocity of carrying away of heat, i.e. the cooling velocity.

All possible cooling velocities are contained between the limits of infinitely large and infinitely small (Fig. 5). The higher limit refers to obtaining glassy microstructures [4], while the lower refers to equilibrium solidification. In real castings solidification proceeds well within these limits, but the cooling velocities can vary widely in any one casting.

Directly taking into account the melt undercooling leads to many numerical complications in the solidification model. Assuming that solidification starts at the liquidus temperature, and that the undercooling quantity, represented by the cooling velocity, decides the characteristic dimension of the created microstructure is a much better solution.

In the paper it was assumed that only one type of microstructure is formed, namely equiaxed microstructure. It was also assumed that the final grain radius is a characteristic dimension, the value of which depends on the cooling velocity according to

$$r_g = r_b\left(1 - \exp\left(-\frac{1}{\dot{T}}\right)\right), \tag{62}$$

where r_b is the maximum grain radius in the calculated microstructure, while $\dot{T}$ is the average cooling velocity, calculated from the beginning of the cooling process till the liquidus temperature is reached. In Eq. (62) the maximum grain radius depends on the constitution of the casting alloy and should be established experimentally. The curve course of the equiaxed grain distribution is

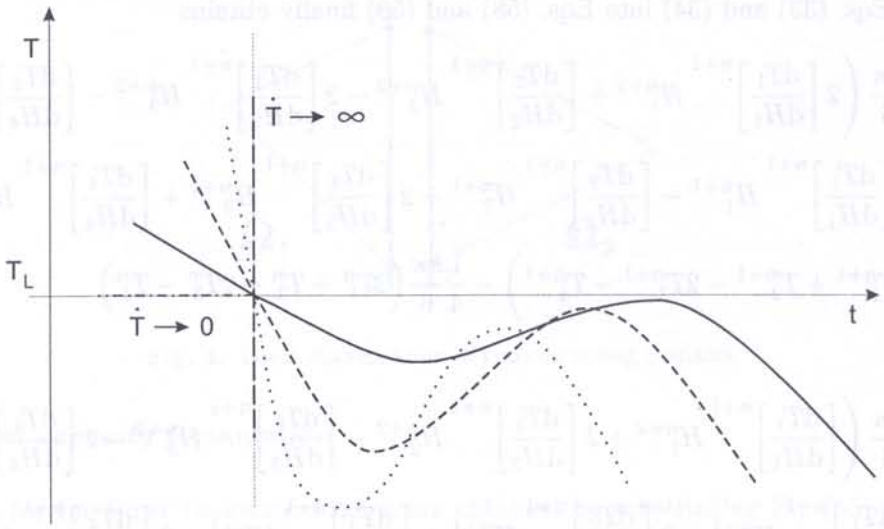

Fig. 5. The cooling curves for different cooling velocities

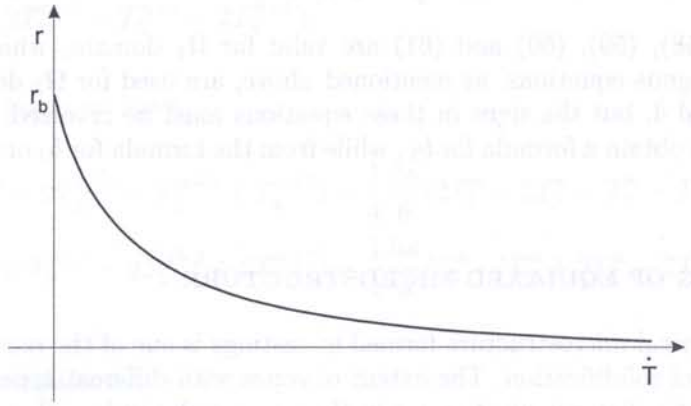

Fig. 6. The relationship of equiaxed grain radius to cooling velocity

in accordance with an experiment [5, 17]. A fine-grained microstructure is received for very large values of undercooling (for high $\dot{T}$ values), including the outer equiaxed grains. The equiaxed grains radii are not much different in the internal regions of the casting, where undercooling is smaller than undercooling in the layers in contact with the mould.

6. Examples of computer simulations

A suitable computer program module was created on the basis of previously conducted object-oriented analysis and previously worked out models of solid phase growth [15], as well on the basis of the numerical models presented in this paper. This module, named *Solidification*, is a part of the *NuscaS* computer program, which has been developed over the past few years by the Institute of Mechanics and Machine Design at the Technical University of Częstochowa. The *NuscaS* program, as well as modules included in it, has been created on the basis of the object-oriented technique.

Examples of computer simulations were carried out for Al – 4,5 % Cu alloy solidifying in a metal mould. The above alloy was chosen because of its wide range of solidification temperatures. The assumed values of the material properties, are taken from work [1], and temperatures, taken from the Al–Cu phase diagram, are shown in Table 1.

Table 1. The material properties

		liquid phase	solid phase	mould
ρ	[kg/m^3]	2500	2800	7200
c	[J/kgK]	1100	900	736
λ	[W/mK]	90	200	24
L	[J/kg]	390000		
T_S	[K]	853		
T_L	[K]	923		
T_E	[K]	821		
T_M	[K]	933		
k		0.125		

It was assumed that the maximum grain radius equals 10^{-3} m. The initial casting (melt) temperature was 960 K, while the initial mould temperature was 660 K. The analysed casting together with the mould, is shown in Fig. 7. The regions were divided into 16 994 triangular finite elements, receiving 9 183 nodes. The chosen nodes, for which cooling curves diagrams were made, are also shown in Fig. 7. The fourth type of boundary condition with non-ideal contact between the casting and the mould was assumed. The conductivity of the separating layer was equal to 1000 W/m^{2}K. The third type of boundary condition was established on the remaining boundaries. It was assumed that the ambient temperature equaled 300 K, while the heat exchange coefficient with the environment equaled 1000 W/m^{2}K. A time step equal to 0.05 s was applied in the calculations. The computer simulations were carried out for linear dependence of enthalpy to temperature [14].

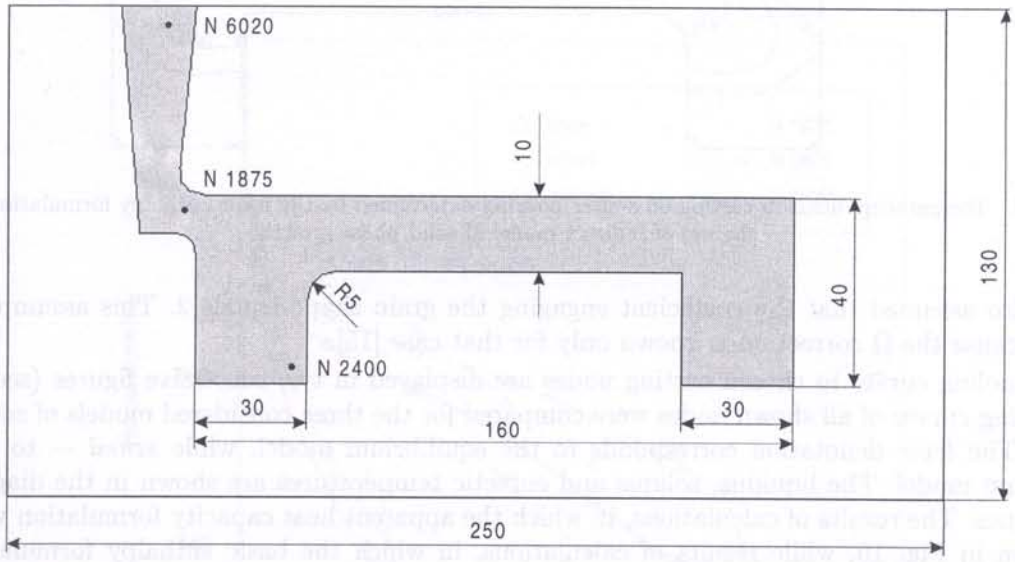

Fig. 7. Analysed casting in mould

The results of computer simulations are shown in the following figures. Figures 8 and 9 illustrate the temperature fields in castings after 30 s and 60 s from the beginning of cooling. The temperature fields in both figures were obtained using the indirect model of solid phase growth, for the apparent heat capacity formulation (Fig. 8) and for the basic enthalpy formulation (Fig. 9). In calculations, where the indirect model of solid phase growth was used, it was assumed that the $D_s t_f$ product (of solute diffusion coefficient in the solid phase and local time of solidification) is equal to $3 \cdot 10^{-9}$ m^2.

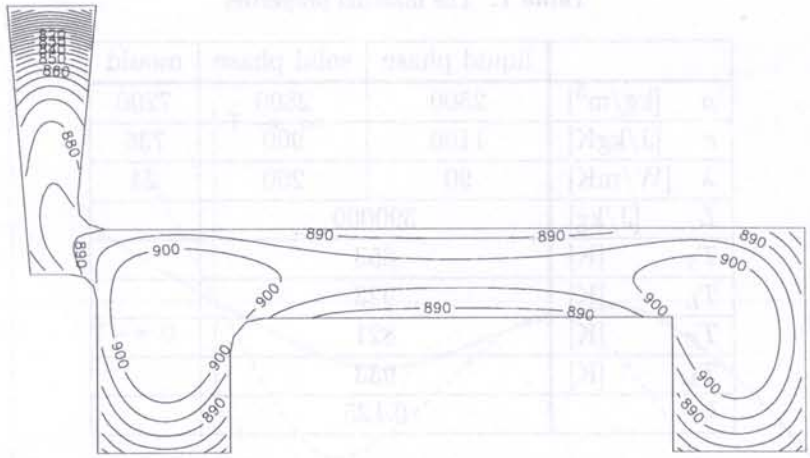

Fig. 8. Temperature fields in casting 30 s after pouring determined by the apparent heat capacity formulation with the use of indirect model of solid phase growth

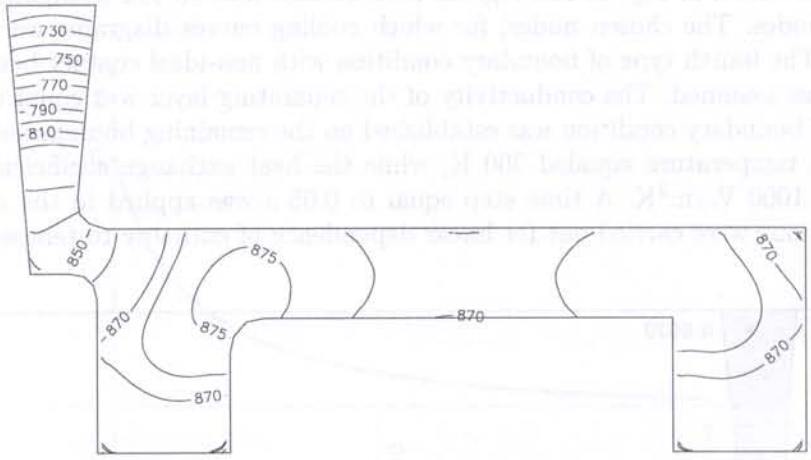

Fig. 9. Temperature fields in casting 60 s after pouring determined by the basic enthalpy formulation with the use of indirect model of solid phase growth

It was also assumed that the coefficient engaging the grain shape equals 2. This assumption was made because the Ω correction is known only for that case [15].

The cooling curves in chosen casting nodes are displayed in two successive figures (see Fig. 7). The cooling curves of all shown nodes were compared for the three considered models of solid phase growth. The *lever* denotation corresponds to the equilibrium model, while *scheil* — to the non-equilibrium model. The liquidus, solidus and eutectic temperatures are shown in the diagrams by dashed lines. The results of calculations, in which the apparent heat capacity formulation was used, are shown in Fig. 10, while results of calculations, in which the basic enthalpy formulation was used, are shown in Fig. 11. For both solidification formulations analysed here the cooling curves are different. It seems that these differences come from the different ways of evaluating systems of equations. In the basic enthalpy formulation the solid phase fraction (exactly talking its derivative) is introduced into the coefficients calculation, while in the apparent heat capacity formulation the calculation of solid phase fraction is a purely postprocessor operation.

The basic enthalpy formulation together with the indirect model of solid phase growth allow the grain sizes to be directly taken into account in the calculations. This is significant because depending on the cooling conditions and grain sizes, the solidification can end either at the eutectic temperature or at a temperature higher than the eutectic one but lower than the equilibrium solidus

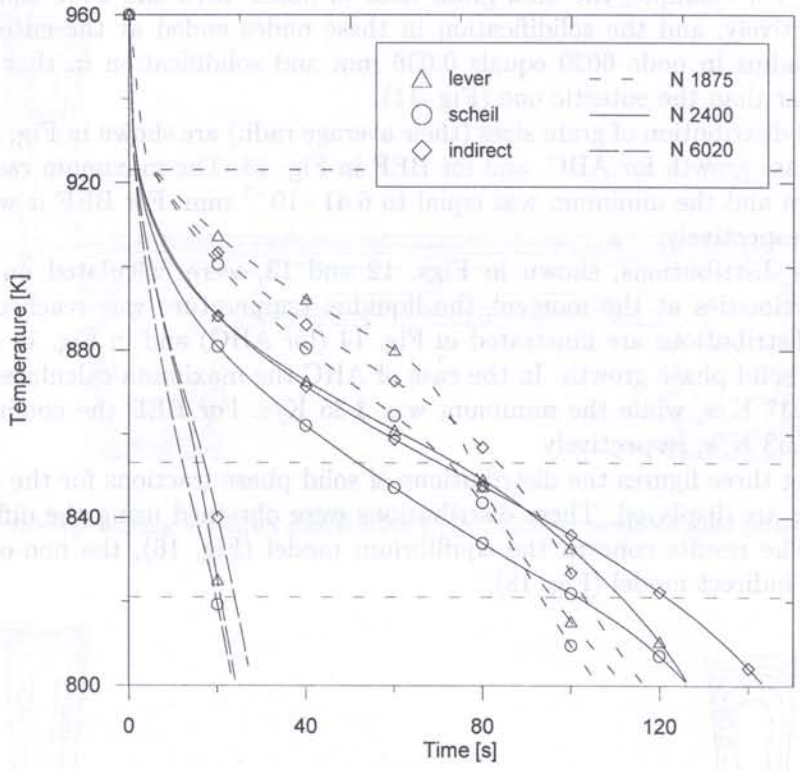

Fig. 10. Cooling curves in chosen casting nodes (apparent heat capacity formulation)

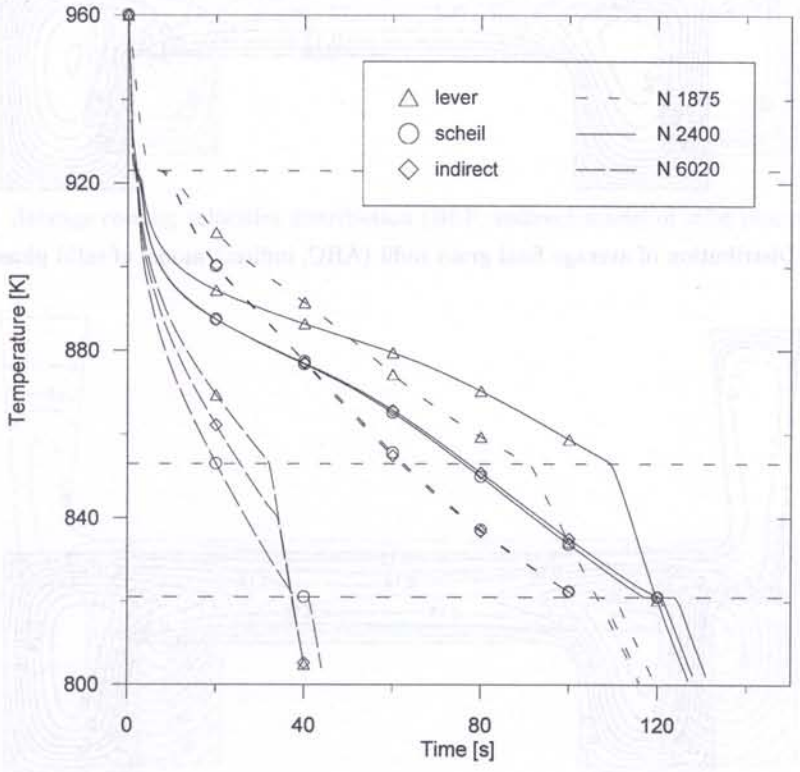

Fig. 11. Cooling curves in chosen casting nodes (basic enthalpy formulation)

temperature [14]. For example, the final grain radii in nodes 1875 and 2400 equal 0.164 mm and 0.067 mm, respectively, and the solidification in these nodes ended at the eutectic temperature. The final grain radius in node 6020 equals 0.036 mm and solidification in that node ended at a temperature higher than the eutectic one (Fig. 11).

The calculated distribution of grain sizes (their average radii) are shown in Fig. 12 for the indirect model of solid phase growth for AHC, and for BEF in Fig. 13. The maximum radius for AHC was equal to 0.258 mm and the minimum was equal to $6.41 \cdot 10^{-3}$ mm. For BEF it was 0.351 mm and $6.42 \cdot 10^{-3}$ mm, respectively.

The grain size distributions, shown in Figs. 12 and 13, were calculated on the basis of the average cooling velocities at the moment the liquidus temperature was reached. The calculated cooling velocity distributions are illustrated in Fig. 14 (for AHC) and in Fig. 15 (for BEF) for the indirect model of solid phase growth. In the case of AHC the maximum calculated cooling velocity was equal to 155.37 K/s, while the minimum was 3.35 K/s. For BEF the cooling velocities were 155.74 K/s and 2.33 K/s, respectively.

In the following three figures the distributions of solid phase fractions for the AHC formulation 30 s after pouring are displayed. These distributions were obtained using the different solid phase growth models. The results concern the equilibrium model (Fig. 16), the non-equilibrium model (Fig. 17) and the indirect model (Fig. 18).

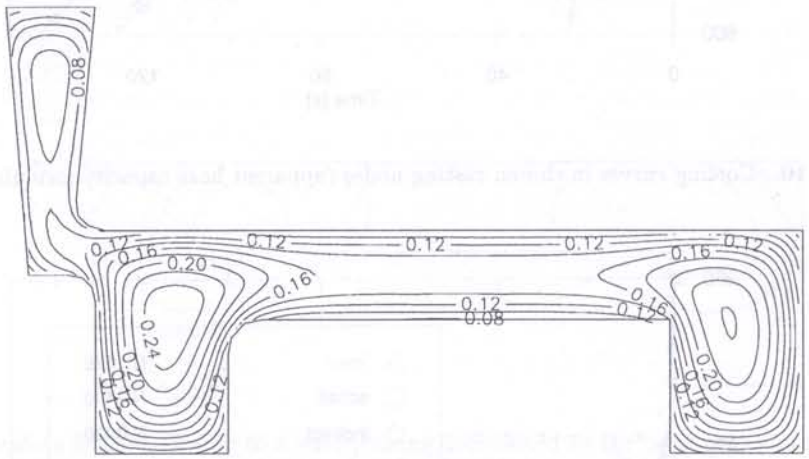

Fig. 12. Distribution of average final grain radii (AHC, indirect model of solid phase growth)

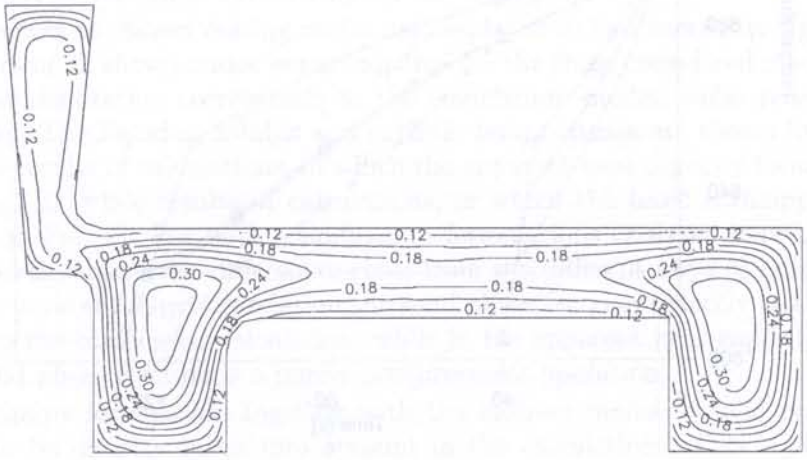

Fig. 13. Distribution of average final grain radii (BEF, indirect model of solid phase growth)

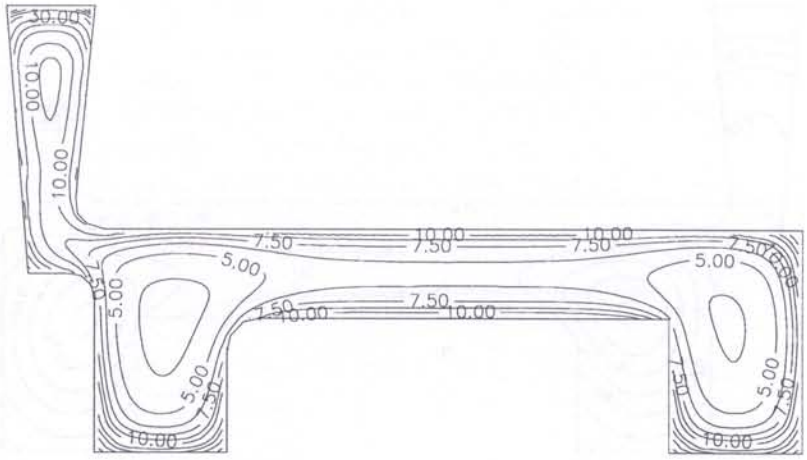

Fig. 14. Average cooling velocities distribution (AHC, indirect model of solid phase growth)

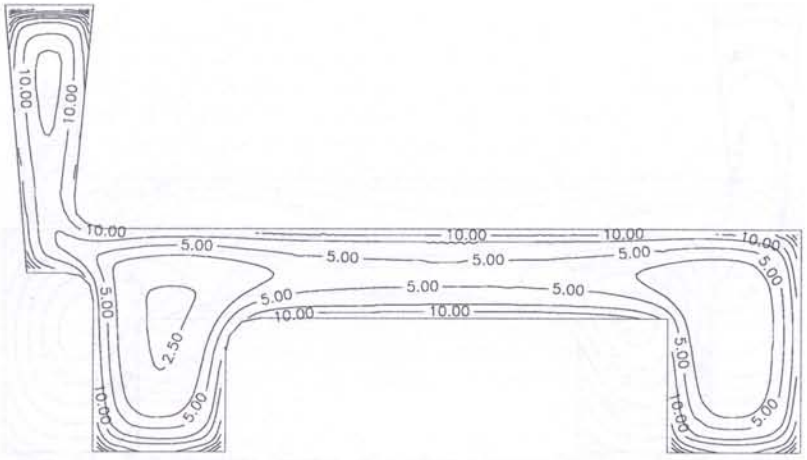

Fig. 15. Average cooling velocities distribution (BEF, indirect model of solid phase growth)

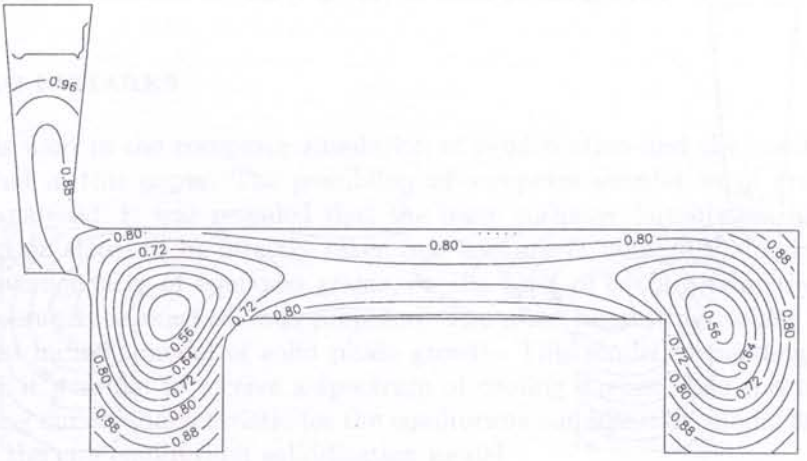

Fig. 16. Solidification kinetics 30 s after pouring (AHC, equilibrium model)

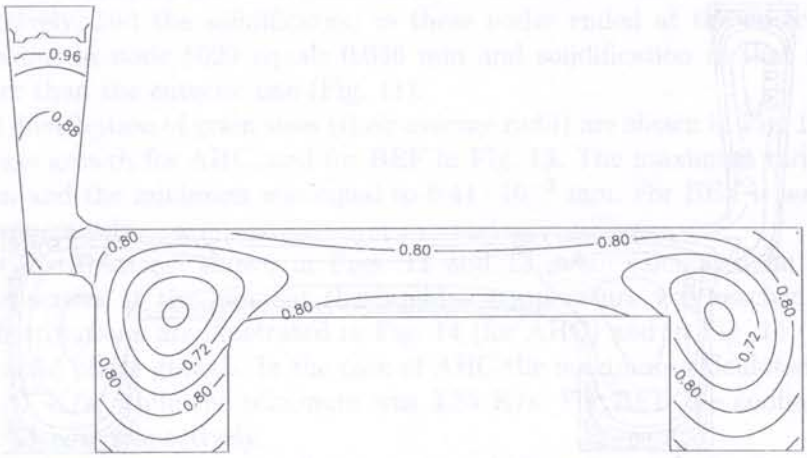

Fig. 17. Solidification kinetics 30 s after pouring (AHC, non-equilibrium model)

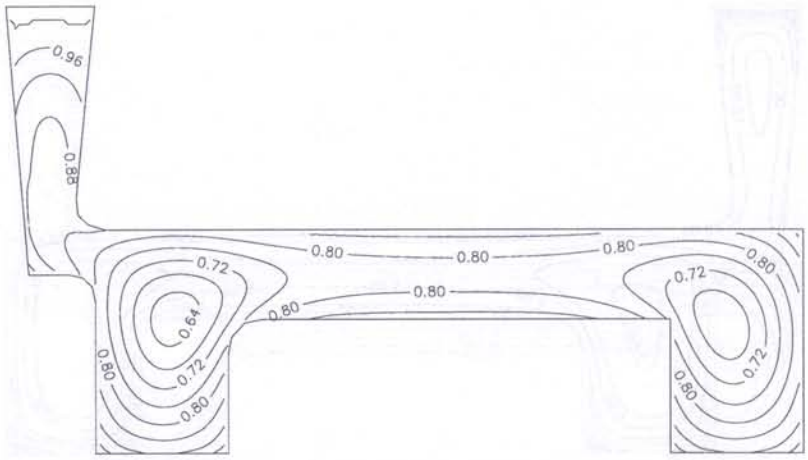

Fig. 18. Solidification kinetics 30 s after pouring (AHC, indirect model)

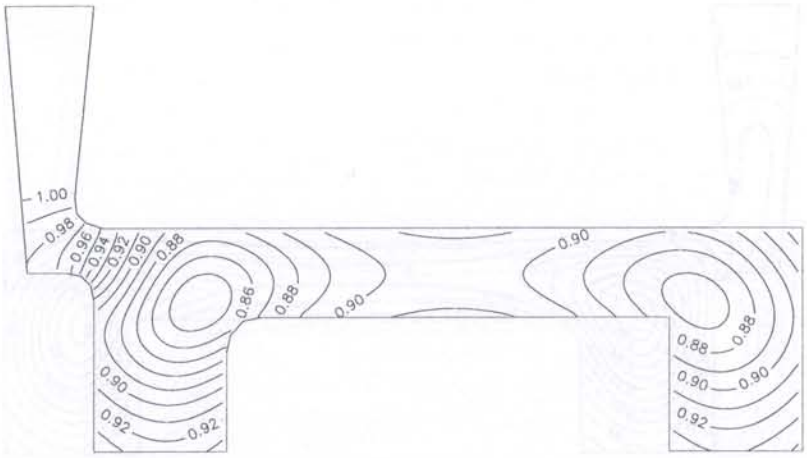

Fig. 19. Solidification kinetics 60 s after pouring (BEF, equilibrium model)

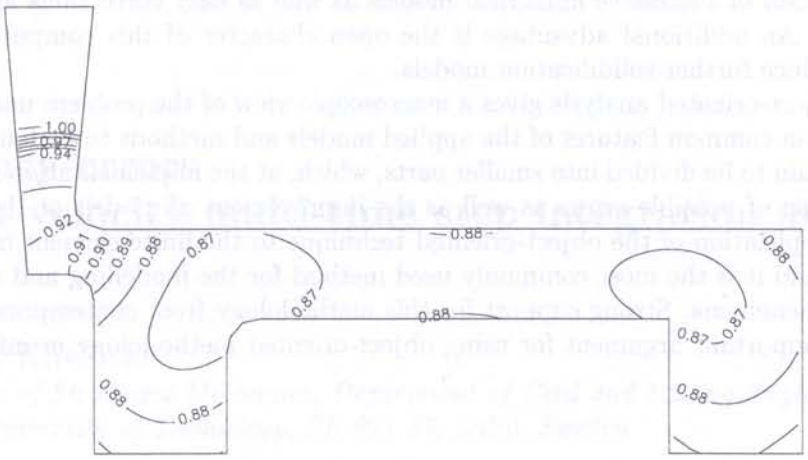

Fig. 20. Solidification kinetics 60 s after pouring (BEF, non-equilibrium model)

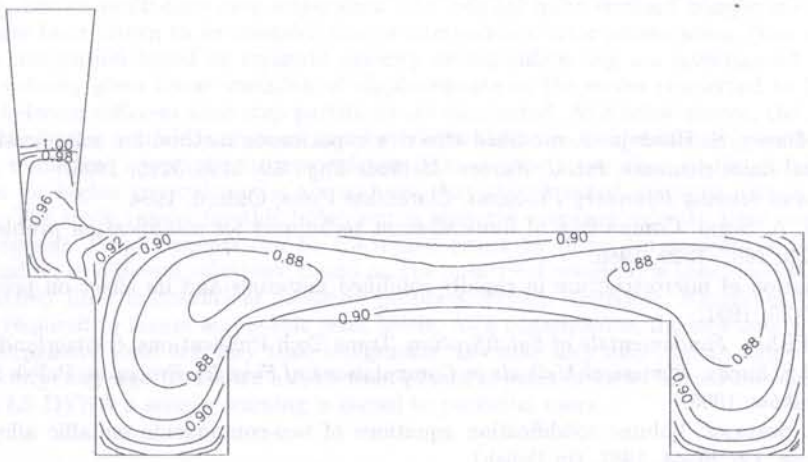

Fig. 21. Solidification kinetics 60 s after pouring (BEF, indirect model)

The analogous comparison for the BEF formulation 60 s after pouring is presented in the last three figures. The results shown there concern the equilibrium model (Fig. 19), the non-equilibrium model (Fig. 20) and the indirect model (Fig. 21) of solid phase growth.

7. Concluding remarks

Numerical models used in the computer simulation of solidification and the results obtained from them are presented in this paper. The possibility of computer simulation of grained microstructure creation is analysed. It was revealed that the basic enthalpy formulation allows the created microstructure (grain sizes) to be directly taken into account in numerical simulations. A method to estimate the average sizes of equiaxed grains, on the basis of cooling velocities at the moment the liquidus temperature is reached, was proposed. The most interesting results were received by using the so-called indirect model of solid phase growth. This model, depending on solidification conditions, makes it possible to receive a spectrum of cooling curves. This spectrum is bound by the limits of cooling curves characteristic for the equilibrium solidification model and cooling curves characteristic for the non-equilibrium solidification model.

The results of computer simulation, presented in this paper, were obtained with the help of a computer program prepared according to object-oriented methodology. Such an approach allows the

easy implementation of successive numerical models as well as easy corrections and improvements to those models. An additional advantage is the open character of this computer program: it is possible to introduce further solidification models.

The use of object-oriented analysis gives a macroscopic view of the problem under consideration and enables certain common features of the applied models and methods to be found. It also allows the problem domain to be divided into smaller parts, which, at the implementation stage, guarantees quicker localisation of possible errors as well as the improvement of models or the introduction of new ones. The application of the object-oriented technique to the finite element method started in the early 90ties and it is the most commonly used method for the modelling and simulation of different physical phenomena. Strong support for this methodology from contemporary programming languages is an important argument for using object-oriented methodology in information system techniques.

Acknowledgement

The current work is sponsored by the State Committee for Scientific Research of the Republic of Poland for 1997–1999 under Grant No. 8 T11F 016 12.

References

[1] S. Bounds, K. Davey, S. Hinduja. A modified effective capacitance method for solidification modelling using linear tetrahedral finite elements. *Int. J. Numer. Methods Eng.*, **39**: 3195–3215, 1996.

[2] J. Crank. *Free and Moving Boundary Problems.* Clarendon Press, Oxford, 1984.

[3] A.J. Dalhuijsen, A. Segal. Comparison of finite element techniques for solidification problems. *Int. J. Numer. Methods Eng.*, **23**: 1807–1829, 1986.

[4] H. Jones. Formation of microstructure in rapidly solidified materials and its effect on properties. *Mater. Sci. Eng.*, **A137**: 77–85, 1991.

[5] W. Kurz, D.J. Fisher. *Fundamentals of Solidification.* Trans Tech Publications, Switzerland, 1989.

[6] B. Mochnacki, J.S. Suchy. *Numerical Methods in Computations of Foundry Processes.* Polish Foundrymen's Tech. Association, Kraków, 1995.

[7] R. Parkitny, N. Sczygiol. Volume solidification equations of two-components metallic alloys. *Solidification of Metals and Alloys*, **12**: 29–44, 1987. (in Polish)

[8] R. Parkitny, N. Sczygiol. Erstarrungsthermomechanik eines Gußstückes unter Berücksichtigung seines Kornaufbaus. *ZAMM*, **69**: T514–T515, 1989.

[9] M. Rappaz, Ch.-A. Gandin. Probabilistic modelling of microstructure formation in solidification processes. *Acta Metall. Mater.*, **41**: 345–360, 1993.

[10] Y. Saad. *Iterative Methods for Sparse Linear Systems.* PWS Publishing, New York, 1995.

[11] N. Sczygiol. Solidification equations by means of finite elements method (in Polish). *Solidification of Metals and Alloys*, **30**: 221–232, 1997.

[12] N. Sczygiol, G. Szwarc, T. Olas, A. Nagórka. Object-oriented analysis of solidification modelled by finite elements (in Polish). *Solidification of Metals and Alloys*, **30**: 233-242, 1997.

[13] N. Sczygiol. Numerical modelling of castings solidification concerning the forming grained microstructure (in Polish). *Archives of Mechanical Technology and Automatization*, **18**: 275–285, 1998.

[14] N. Sczygiol. Approaches to enthalpy approximation in numerical simulation of two-component alloy solidification. *Computer Assisted Mechanics and Engineering Sciences*, **7**: 717–734, 2000.

[15] N. Sczygiol. Object-oriented analysis of the numerical modelling of castings solidification. *Computer Assisted Mechanics and Engineering Sciences*, **8**: 79–98, 2001.

[16] K.K. Tamma, R.R. Namburu. Recent advances, trends and new perspectives via enthalpy-based finite element formulations for applications to solidification problems. *Int. J. Numer. Methods Eng.*, **30**: 803–820, 1990.

[17] Ph. Thvoz, J.L. Desbiolles, M. Rappaz. Modeling of equiaxed microstructure formation in casting. *Metall. Trans. A*, **20A**: 311–322, 1989.

[18] V.R. Voller, C.R. Swaminathan, B.G. Thomas. Fixed grid techniques for phase change problems: a review. *Int. J. Numer. Methods Eng.*, **30**: 875–898, 1990.

[19] W.L. Wood. *Practical Time-stepping Schemes.* Clarendon Press, Oxford, 1990.